Available online at www.sciencedirect.com
ScienceDirect
Journal of the European Ceramic Society 30 (2010) 307–313
www.elsevier.com/locate/jeurceramsoc

# Phase formation and dielectric properties of $Ln_2(Ln'_{0.5}Nb_{0.5})_2O_7$ (Ln = rare earth element)

Lu Cai *, Juan C. Nino

*Department of Materials Science and Engineering, University of Florida, Gainesville, FL 32611, United States*

Available online 24 June 2009

**Abstract**

Weberites and pyrochlores ($A_2B_2O_7$), both fluorite-related superstructures, are attractive dielectric ceramics due to their ability to accommodate diverse cations, thus allowing their properties to be tailored. This study focuses on the fundamental understanding of the structure–dielectric property relationships in fluorite-related oxides. Specifically, $Ln_3NbO_7$ and $Ln_2(Ln'_{0.5}Nb_{0.5})_2O_7$ (where the ionic radius of Ln′ is smaller than that of Ln) compounds are investigated. It has been previously shown that weberite-type $Ln_3NbO_7$ exhibits a composition dependent dielectric relaxation above room temperature. It is here shown that a dielectric relaxation also occurs in $La_2(Ln'_{0.5}Nb_{0.5})_2O_7$ (Ln′ = $Yb^{3+}$, $Er^{3+}$, and $Dy^{3+}$) compounds near or below −158 °C. The temperature, at which the maximum permittivity occurs, is different for different compositions (−132 °C for $La_2(Yb_{0.5}Nb_{0.5})_2O_7$, −197 °C for $La_2(Er_{0.5}Nb_{0.5})_2O_7$, and −187 °C for $La_2(Dy_{0.5}Nb_{0.5})_2O_7$ at 1 MHz) and is correlated with the distortion of the $NbO_6$ octahedra. The room temperature dielectric permittivity of all three compounds was measured to be between 40 and 50 at 1 MHz.


*Keywords:* Dielectric properties; Relaxation

## 1. Introduction

The weberite and the pyrochlore ($A_2B_2O_7$) are both anion-deficiency fluorite ($AO_2$ or $A_4O_8$) superstructures. These two structures have a similar cationic sublattice, which is comprised by the stacking of cubic close-packed cation layers, the same as {1 1 1} planes in the fluorite. These layers alternate between the compositions $A_3B$ and $AB_3$ and are parallel to {1 1 1} planes in the pyrochlore and {0 1 1} planes in the weberite. The crystallographic relationship between the orthorhombic weberite and the cubic pyrochlore is further clarified by the fact that the space group of weberite (*Imma*) is a subgroup of *Fd*-3*m*, the space group of pyrochlore. These two structures can be described as a network of corner-shared $BO_6$ octahedra. However, a significant difference between the two is that all of the oxygen ions in weberites participate in the formation of $BO_6$ octahedra, but only 6 out of 7 oxygen ions participate in pyrochlore structures (see Fig. 1).[1]

The field existence and stability of pyrochlores can typically be predicted based on the ratio of cation ionic radii $R_A/R_B$. For $A_2^{3+}B_2^{4+}O_7$ pyrochlores, the field existence and stability is in the range of $1.46 < R_A/R_B < 1.80$, where $R$ is the ionic radius of the cation.[2] $Ln_2(Ln_{0.5}Nb_{0.5})_2O_7$ ($Ln_3NbO_7$, Ln = $La^{3+}$, $Nd^{3+}$ or $Gd^{3+}$) compounds, which have been reported as weberite-type structures, are not within the pyrochlore stability field.[3–6] By contrast, $Ln_2(Ln'_{0.5}Nb_{0.5})_2O_7$ compounds, where the ionic radius of Ln′ is smaller than that of Ln, lie in or close to the stability area, and thus, as suggested by Isupov,[7] $Ln_2(Ln'_{0.5}Nb_{0.5})_2O_7$ are expected to crystallize in the pyrochlore structure. Therefore, to test this prediction and further understand fluorite-related superstructures, the structure of the three compounds, $La_2(Yb_{0.5}Nb_{0.5})_2O_7$, $La_2(Er_{0.5}Nb_{0.5})_2O_7$ and $La_2(Dy_{0.5}Nb_{0.5})O_7$, were studied here.

In terms of dielectric properties, it has been reported that weberite-type $Ln_3NbO_7$ exhibits a composition dependent dielectric relaxation above room temperature.[8–10] The relaxation temperatures are different, 47 °C, 97 °C, and 197 °C for $Gd_3NbO_7$, $La_3NbO_7$ and $Nd_3NbO_7$, respectively. It has been proposed that different relaxation temperatures may be correlated with polyhedral distortion in the crystal structure of weberite-type $Ln_3NbO_7$. To explore more on the origin of this dielectric relaxation, the dielectric properties of $La_2(Ln_{0.5}Nb_{0.5})_2O_7$ (Ln = $Dy^{3+}$, $Er^{3+}$, and $Yb^{3+}$) are here investigated. This study points to the possibility of tailoring the relaxation in the fluorite-related structures via distortion of the $NbO_6$ octahedra.

* Corresponding author. Tel.: +1 352 2730268; fax: +1 352 8463355.
*E-mail address:* lclisa3@ufl.edu (L. Cai).

0955-2219/$ – see front matter © 2009 Elsevier Ltd. All rights reserved.
doi:10.1016/j.jeurceramsoc.2009.05.026

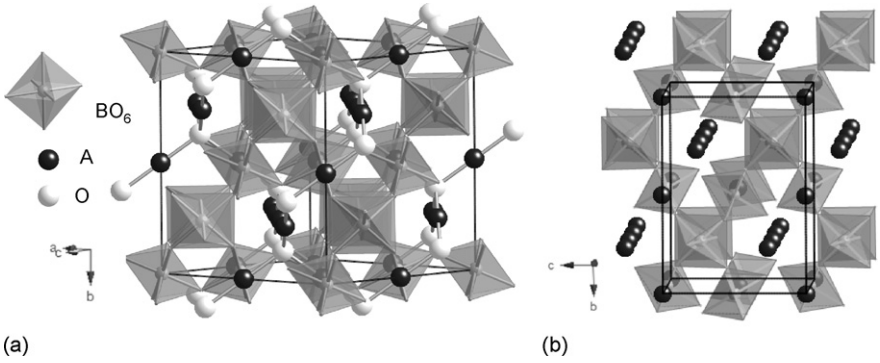


Fig. 1. $BO_6$ polyhedral view of (a) the pyrochlore and (b) the weberite. The line is the unit cell.

## 2. Experimental procedure

Polycrystalline specimens were prepared by solid state processing. The starting materials were $Dy_2O_3$ (Alfa, 99.99%), $Er_2O_3$ (Alfa, 99.99%), $La_2O_3$ (Alfa, 99.99%),$Yb_2O_3$ (Alfa, 99.9%) and $Nb_2O_5$ (Alfa, 99.9985%). A stoichiometric mixture of 20 g $Ln_2O_3$ and $Nb_2O_5$ was combined with 70 ml deionized water and 2 ml ammonium polyacrylate dispersant (Darvan 821 A). The slurry was ball-milled for 24 h, subsequently dried in the oven at 120 °C for 16 h, then ground and sieved through a 212 μm mesh. The powder was then placed in an alumina crucible and calcined at 1400–1500 °C. X-ray diffraction (XRD) was performed to verify phase formation using $CuK_\alpha$ radiation at room temperature. The resulting XRD patterns were compared with the XRD profiles of stoichiometric mixture of unreacted precursors and the JCPDS PDF of all other possible compositions of rare earth niobates such as $LaNbO_4$. Multiple calcinations were performed to ensure phase purity. Between each calcination stages, the powders were finely reground with mortar and pestle.

After calcination, 1–3 wt.% of PVA binder (Celvol 103) was added to assist in pellet formation. Pellets were uniaxially pressed at 150 MPa into cylindrical pellets, 3 mm in diameter and approximately 1.5 mm thick. Pellets were sintered at 1600 °C for 8 h following a binder burnout at 450 °C for 2 h. For dielectric measurements, parallel plate capacitors were made by sputtering Au/Pd electrodes on both sides of the pellets followed by a hand-painted coat of Ag-paste that was dried in air. Dielectric properties were measured using an Agilent 4284A LCR meter over the frequency range of 10 kHz–1 MHz. The measurements were performed in the temperature range of −253 °C to 22 °C with samples in a closed cycle cryogenic workstation (CTI - Cryogenics, Model 22). The measurements were conducted both on cooling and heating.

## 3. Results and discussion

### 3.1. Crystal structure

The XRD profiles of $La_2(Yb_{0.5}Nb_{0.5})_2O_7$ at different calcination temperatures and the stoichiometric mixture of the $La_2O_3$, $Yb_2O_3$ and $Nb_2O_5$ are shown in Fig. 2(a). After initial calcination at 1400 °C for 8 h, the resulting pattern showed a mixture phase of $La_2(Yb_{0.5}Nb_{0.5})_2O_7$, $Yb_3NbO_7$, and $La_2O_3$. After the subsequent calcination at 1500 °C for 24 h, there was no obvious $La_2O_3$ phase, and the $Yb_3NbO_7$ phase was greatly depressed, which relative intensity of the strongest peak decreased from 42% to 7%. After the third calcination at 1500 °C for 24 h, it was clearly shown that there are no unreacted $La_2O_3$, $Yb_2O_3$, $Nb_2O_5$ or $Yb_3NbO_7$ in the $La_2(Yb_{0.5}Nb_{0.5})_2O_7$ pattern. The XRD profile remained the same after additional calcination at 1500 °C for 12 h. Therefore, equilibrium was presumed after the third calcination. Initial inspection of the XRD pattern showed the five characteristic cubic fluorite reflections with $2\theta$ ranging from 10° to 70°. However, upon further analysis, it was observed that several of the five peaks were in fact split into two reflections. The pattern also contained several weak peaks with intensities below 5% relative intensity (Fig. 2(b) and (c)).

Pseudo-Voigt functions were used to fit the diffraction peaks and extract the peak positions using Xfit program.[11] It was observed that the peak splitting did not increase with increasing $2\theta$, which ruled out the possibility of the formation of two fluorite phases. The peak positions were input into Crysfire using Treor program (an indexing program that searches for solutions by varying Miller indices in a trial-and-error manner).[12] The best solution obtained by Treor was an orthorhombic unit cell. The lattice parameters were further refined using Checkcell program.[13] The initial lattice parameters corresponded to an orthorhombic fluorite-related lattice ($\sqrt{2}a$, $2a$ and $\sqrt{2}a$, where $a \sim 5$ Å)[14,15] and therefore, the XRD profile of $La_2(Yb_{0.5}Nb_{0.5})_2O_7$ was then compared with the XRD of fluorite-related structures including orthorhombic pyrochlore, weberite, weberite-type, orthorhombic fluorite, and zirconolite. The XRD pattern of $La_2(Yb_{0.5}Nb_{0.5})_2O_7$ was consistent with that of an orthorhombic pyrochlore structure (e.g. $Cd_2Nb_2O_7$, space group *Ima*2). Therefore, the structural parameters of orthorhombic $Cd_2Nb_2O_7$[16] were used as initial guess for the Rietveld refinement of $La_2(Yb_{0.5}Nb_{0.5})_2O_7$ using Maud program[17]; the lattice parameters were refined to be 7.5623(13) Å, 10.766(2) Å, 7.6619(3) Å. While all experimental peaks can be assigned to the phase, the peaks with relative intensities larger than 4% are indexed and the others below 4% are indicated by diamond symbols in Fig. 2(b).

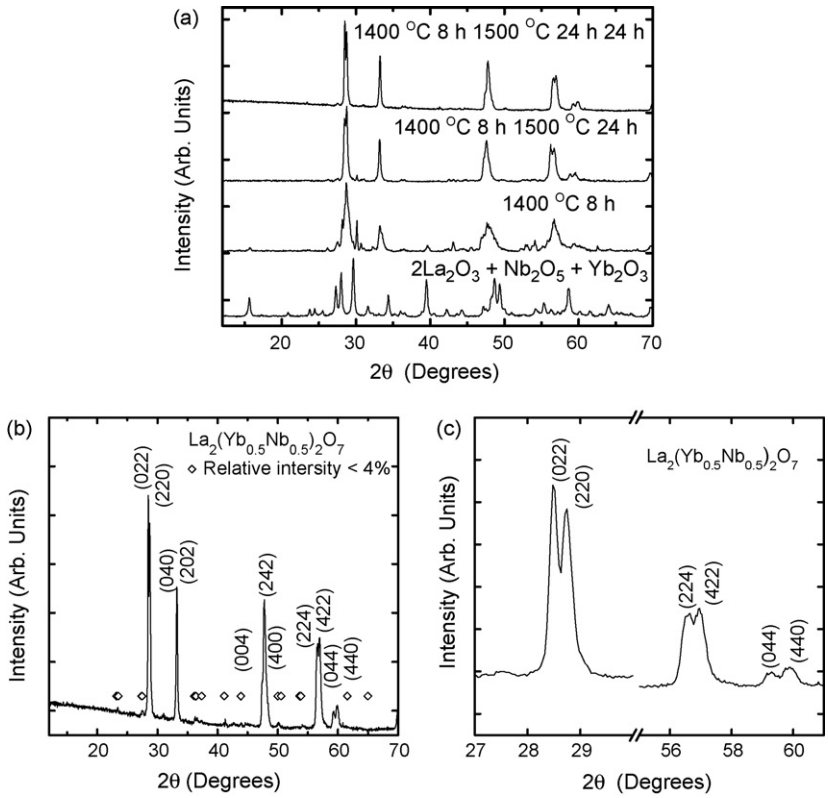


Fig. 2. (a) XRD patterns $La_2(Yb_{0.5}Nb_{0.5})_2O_7$ at different calcination temperatures and time and the mixture of $La_2O_3$, $Nb_2O_5$ and $Yb_2O_3$. (b) Indexed XRD profile of $La_2(Yb_{0.5}Nb_{0.5})_2O_7$ after calcinations at 1400 °C for 8 h and 1500 °C for 24 h and 24 h. (c) Details of the peak splitting in $La_2(Yb_{0.5}Nb_{0.5})_2O_7$.

The XRD profiles of $La_2(Dy_{0.5}Nb_{0.5})_2O_7$ and $La_2(Er_{0.5}Nb_{0.5})_2O_7$ are shown in Fig. 3. The 5 characteristic fluorite peaks were all split into two or more peak reflections. The patterns contained more weak peaks than in the case of $La_2(Yb_{0.5}Nb_{0.5})_2O_7$. Similar XRD analysis as described above was performed on the XRD profiles of $La_2(Dy_{0.5}Nb_{0.5})_2O_7$ and $La_2(Er_{0.5}Nb_{0.5})_2O_7$. In both cases, the minor peaks at $2\theta \sim 26^\circ$, 29.5° and 31° could not be indexed based on an orthorhombic pyrochlore. However, the XRD patterns were found to be consistent with the weberite-type structure (e.g. $Nd_3NbO_7$, space group *Cmcm*).[3] Rietveld refinement of $La_2(Dy_{0.5}Nb_{0.5})_2O_7$ and $La_2(Er_{0.5}Nb_{0.5})_2O_7$ was thus based on the structure of $Nd_3NbO_7$. The lattice parameters of $La_2(Dy_{0.5}Nb_{0.5})_2O_7$ are 10.921(2) Å, 7.5646(12) Å and 7.7060(13) Å. The lattice parameters of $La_2(Er_{0.5}Nb_{0.5})_2O_7$ are 10.9220(8) Å, 7.5915(12) Å and 7.7189(5) Å. While all observed peaks can be assigned to the phases, the peaks with relative intensities larger than 8% are indexed and the other less intense peaks are indicated by diamond symbols in Fig. 3. The summary of lattice parameters is listed in Table 1.

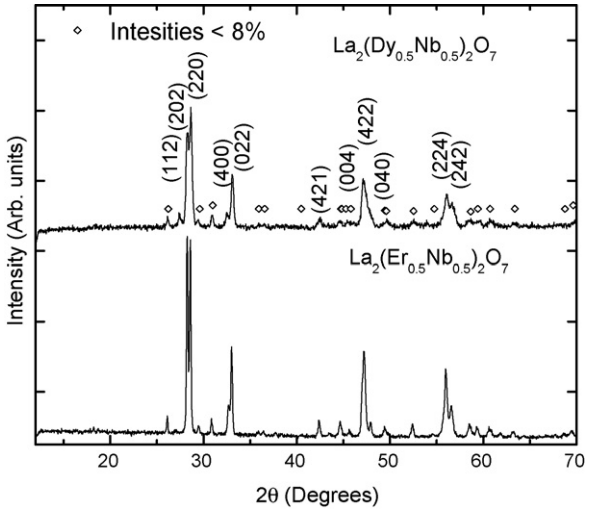


Fig. 3. XRD patterns of $La_2(Dy_{0.5}Nb_{0.5})_2O_7$ and $La_2(Er_{0.5}Nb_{0.5})_2O_7$.

### 3.2. Dielectric properties

The dielectric measurements have been performed both on cooling and on heating in the temperature range of −253 °C–22 °C. It is important to note that dielectric data measured on cooling matches well with that on heating for all the compounds. The dielectric behavior of $La_2(Yb_{0.5}Nb_{0.5})_2O_7$ as a function of temperature at the frequencies from 10 kHz to 1 MHz is shown in Fig. 4. The real part of permittivity is between 43.5 and 44.5 from −253 °C to 22 °C, and the imaginary part of permittivity is on the order of $10^{-1}$ at 1 MHz. It is observed that the dielectric behavior undergoes a frequency and temperature dependent dielectric relaxation. The permittivity increases slightly with increasing temperature from −253 °C to about −133 °C where a maximum is reached (∼44.5 at 1 MHz). The temperature, where the maximum permittivity occurs, and consequently the temperature

Table 1
Summary of lattice parameters and the temperature where the maximum of the permittivity occurs ($T(\varepsilon_m)$).

| Compound | $a$ (Å) | $b$ (Å) | $c$ (Å) | Unit cell volume (Å$^3$) | $T(\varepsilon_m)$ |
|---|---|---|---|---|---|
| $Nd_3NbO_7$ | 10.8606(17) | 7.5122(10) | 7.5973(9) | 619.8409 | 204 °C |
| $La_3NbO_7$ | 11.1798(19) | 7.6562(11) | 7.7757(11) | 665.5594 | 90 °C |
| $Gd_3NbO_7$ | 10.6114(5) | 7.5202(4) | 7.5393(3) | 601.6350 | 48 °C |
| $La_2(Yb_{0.5}Nb_{0.5})_2O_7$ | 7.5623(13) | 10.766(2) | 7.6619(13) | 623.8339 | −132 °C |
| $La_2(Er_{0.5}Nb_{0.5})_2O_7$ | 10.9220(8) | 7.5915(5) | 7.7189(5) | 640.0076 | −197 °C |
| $La_2(Dy_{0.5}Nb_{0.5})_2O_7$ | 10.921(2) | 7.5646(12) | 7.7060(13) | 636.6158 | −187 °C |

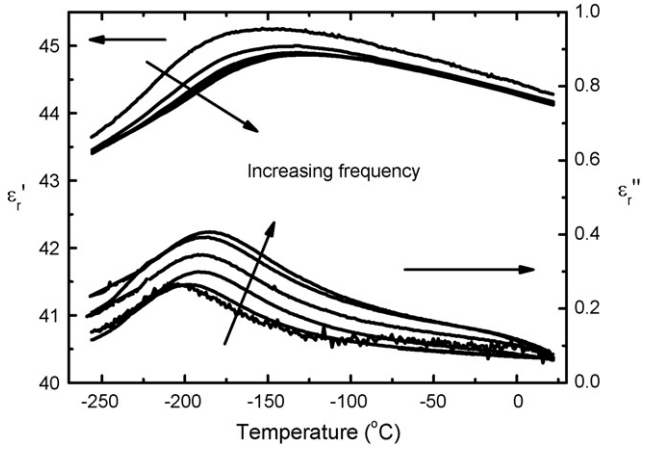


Fig. 4. Dielectric properties of $La_2(Yb_{0.5}Nb_{0.5})_2O_7$ at 10 kHz, 100 kHz, 300 kHz, 500 kHz, 800 kHz and 1 MHz.

($T_m$), where the peak of the imaginary part of permittivity is located, both increase with increasing frequency. However, the dielectric relaxation behavior of $La_2(Yb_{0.5}Nb_{0.5})_2O_7$ is different from that observed in weberite-type $Gd_3NbO_7$.[9] In $Gd_3NbO_7$, there is no clear shift in the maxima of the dielectric permittivity and a larger variation of $T_m$ as a function of frequency.

To better understand the phenomena, as customarily, the Arrhenius function is used to model the relaxation behavior of $La_2(Yb_{0.5}Nb_{0.5})_2O_7$:

$$\nu = \nu_0 \exp\left[-\frac{E_a}{K_B T_m}\right] \quad (1)$$

where $\nu$ is the frequency, the pre-exponential $\nu_0$ is the attempt jump frequency, $E_a$ is the activation energy, and $k_B$ is Boltzmann's constant. The resulting Arrhenius plot is presented in Fig. 5. From the linear fit, $\nu_0 = 1.2 \times 10^{14}$ Hz, and the activation energy $E_a$ is 0.14 eV. The attempt frequency is lower than cubic pyrochlore CaO-$TiO_2$-$Nb_2O_5$ ($4.6 \times 10^{14}$ Hz), but higher than pyrochlore $Bi_{1.5}ZnNb_{1.5}O_7$ ($3 \times 10^{12}$ Hz).[18,19] It is proposed that lighter $A$ site cations result in a higher attempt frequency because the attempt frequency is related to that of O′-$A$-O′ bending phonon mode.[18,20] The calculated attempt frequency of $La_2(Yb_{0.5}Nb_{0.5})_2O_7$ is also acceptable as the mass of $A$ cations ($La^{3+}$) is intermediate among these three compounds. The observed activation energy is smaller than that of weberite-type $Gd_3NbO_7$, 0.45 eV and close to $B_{1.5}ZnNb_{1.5}O_7$, 0.136 eV.[9,19]

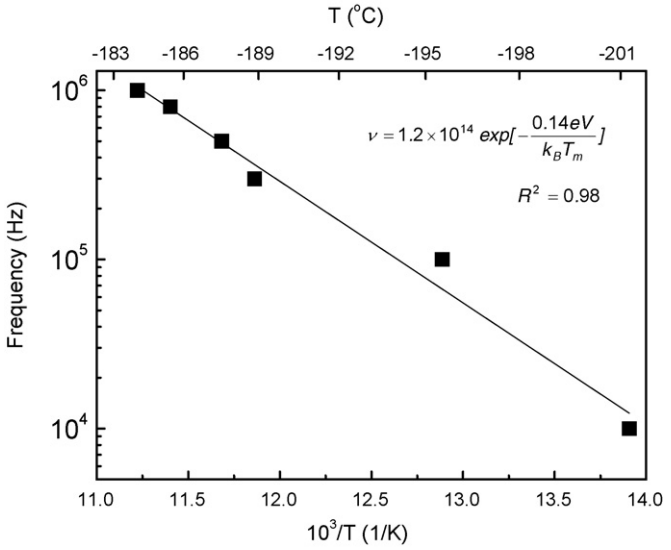


Fig. 5. Arrhenius plot of temperature at which the maximum of imaginary parts of permittivity occurs for $La_2(Yb_{0.5}Nb_{0.5})_2O_7$.

The dielectric properties of $La_2(Dy_{0.5}Nb_{0.5})_2O_7$ are shown in Fig. 6. The permittivity slightly increases from 54.9 to 55.2 from −248 °C to −187 °C, and then decreases to 51 at room temperature at 1 MHz. The imaginary part of permittivity is on the order of $10^{-1}$ at 1 MHz, the same as the other two compounds. This compound also exhibits a dielectric relaxation. The maximum of the permittivity shifts to a higher temperature with increasing frequency. The Arrhenius function is also used

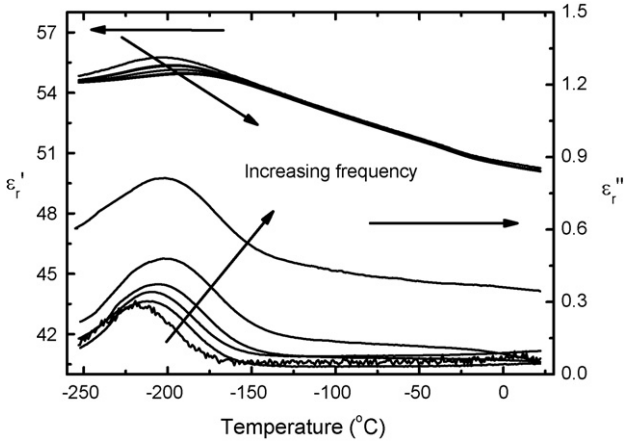


Fig. 6. Dielectric properties of $La_2(Dy_{0.5}Nb_{0.5})_2O_7$ at 10 kHz, 100 kHz, 300 kHz, 500 kHz, 800 kHz and 1 MHz.

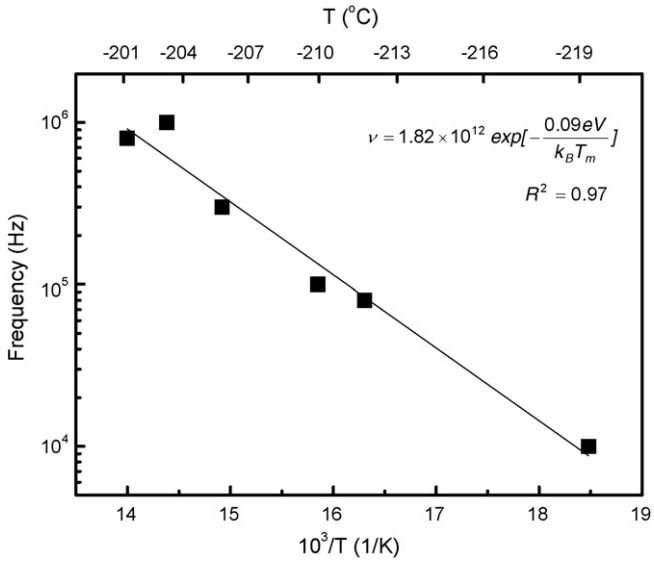


Fig. 7. Arrhenius plot of temperature at which the maximum of imaginary parts of permittivity occurs for $La_2(Dy_{0.5}Nb_{0.5})_2O_7$.

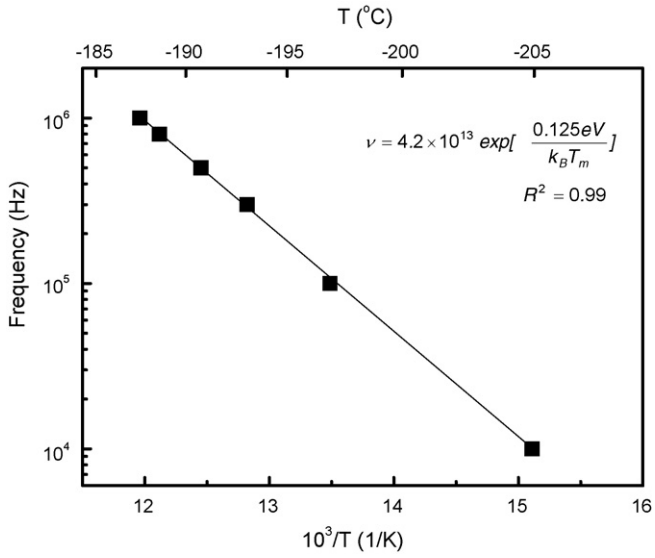


Fig. 9. Arrhenius plot of temperature at which the maximum of imaginary parts of permittivity occurs for $La_2(Er_{0.5}Nb_{0.5})_2O_7$.

to model the relaxation behavior of $La_2(Dy_{0.5}Nb_{0.5})_2O_7$. The resulting Arrhenius plot is presented in Fig. 7. From the linear fit, $\nu_0 = 1.82 \times 10^{12}$ Hz, and the activation energy $E_a$ is 0.09 eV. The attempt frequency of $La_2(Dy_{0.5}Nb_{0.5})_2O_7$ is on the same order of that of cubic pyrochlore $Bi_{1.5}ZnNb_{1.5}O_7$ ($3 \times 10^{12}$ Hz).[19] The activation energy is below those of $Bi_{1.5}ZnNb_{1.5}O_7$, $La_2(Yb_{0.5}Nb_{0.5})_7$ and $Gd_3NbO_7$.[9,19] While this compound is neither, a dipolar glass or relaxor ferroelectric, it is important to note that similar activation energies have been observed or calculated for those type of materials, and thus the measured activation energy value (0.09 eV) is not unheard of.[21–23]

Fig. 8 shows the dielectric properties for $La_2(Er_{0.5}Nb_{0.5})_2O_7$ as a function of temperature at different frequencies from 10 kHz to 1 MHz. The permittivity is between 48 and 50.4 from −253 °C to 22 °C, and the imaginary part of permittivity is also on the order of $10^{-1}$ at 1 MHz. This compound also exhibits a frequency and temperature dependent dielectric relaxation. The real part of permittivity of $La_2(Er_{0.5}Nb_{0.5})_2O_7$ at different frequencies becomes more dispersive near the relaxation temperature while above −123 °C, the variation of permittivity as a function of frequency is negligible. At the same time, the variation of the real part of permittivity as a function of temperature near the relaxation temperature is smaller than that from room temperature to −173 °C. There is no clear shift in the maxima of the dielectric permittivity with respect to frequency in $La_2(Er_{0.5}Nb_{0.5})_2O_7$, which is similar to $Gd_3NbO_7$.[9] $T_m$ increases with increasing frequency from 10 kHz to 1 MHz. The Arrhenius function is also used to model the relaxation behavior of $La_2(Er_{0.5}Nb_{0.5})_2O_7$ as shown in Fig. 9. The calculated $\nu_0$ is $4.2 \times 10^{13}$ Hz, and the activation energy $E_a$ is 0.125 eV. These two values are close to those of $La_2(Yb_{0.5}Nb_{0.5})_2O_7$.

### 3.3. Structure–property relationship

It has been shown in the past that different degrees of polyhedral distortion in $LnO_8$ and $NbO_6$ correlate well with the

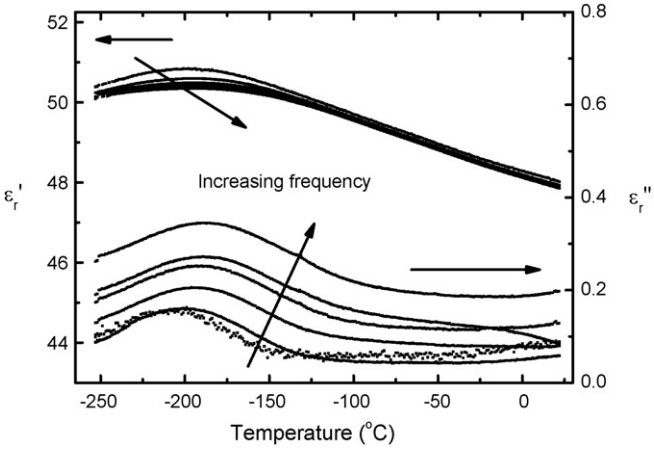


Fig. 8. Dielectric properties of $La_2(Er_{0.5}Nb_{0.5})_2O_7$ from 10 kHz to 1 MHz.

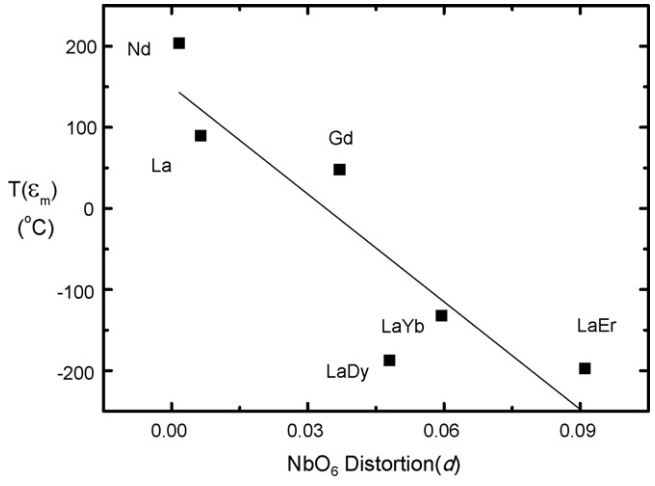


Fig. 10. $NbO_6$ octahedra distortion ($d$) vs. $T(\varepsilon_m)$.

different relaxation temperatures ($T(\varepsilon_m)$, the temperature where maximum real parts of permittivity occurs) in weberite-type $Ln_3NbO_7$.[1,8] Here, it may be possible that the polyhedral distortion can also explain the origin of different dielectric relaxation temperatures in $La_2(Ln'_{0.5}Nb_{0.5})_2O_7$ (the summary of $T(\varepsilon_m)$ is listed in Table 1). The distortion index by Baur[24] were used to characterize the polyhedral distortion:

$$\text{Distortion } (d) = \frac{1}{n}\sum_{i=1}^{n}\frac{|d_i - d_{ave}|}{d_{ave}} \quad (2)$$

where in $MO_n$ polyhedra, $d_i$ is the polyhedral edge length (O–O) and $d_{ave}$ is the average polyhedral edge length. The polyhedral characterization is focused on $NbO_6$ octahedra since weberite-type $Ln_3NbO_7$ and $La_2(Ln_{0.5}Nb)_2O_7$ have common Nb sublattice (or $NbO_6$ octahedra). It is found out the distortion of $NbO_6$ may closely relate to the dielectric properties. As shown in Fig. 10, $T(\varepsilon_m)$ at 1 MHz decreases with increasing distortion ($d$) of $NbO_6$ with exception of $La_2(Dy_{0.5}Nb_{0.5})_2O_7$ (the line is for visual aid). The $NbO_6$ distortion may be attributed to the "openness" of the structure which causes an easier polarization of the material and thus lower $T(\varepsilon_m)$.[8,10] The attributed "openness" can be easily observed by comparing $La_2(Er_{0.5}Nb_{0.5})_2O_7$ and $La_2(Dy_{0.5}Nb_{0.5})_2O_7$. $La_2(Er_{0.5}Nb_{0.5})_2O_7$ has a larger unit cell volume than $La_2(Dy_{0.5}Nb_{0.5})_2O_7$ though the ionic radius of $Er^{3+}$ (0.890 Å) is smaller than that of $Dy^{3+}$ (0.912 Å).[25] The larger unit cell volume of $La_2(Er_{0.5}Nb_{0.5})_2O_7$ is probably contributed by the greater $NbO_6$ distortion. Therefore, $La_2(Er_{0.5}Nb_{0.5})_2O_7$ has a slightly lower $T(\varepsilon_m)$ (−197 °C) than that of $La_2(Dy_{0.5}Nb_{0.5})_2O_7$ (−187 °C). However, $La_2(Yb_{0.5}Nb_{0.5})_2O_7$ has a greater $NbO_6$ distortion than that of $La_2(Dy_{0.5}Nb_{0.5})_2O_7$, but $La_2(Yb_{0.5}Nb_{0.5})_2O_7$ has a higher $T(\varepsilon_m)$. If considered from normalized unit cell volume ($V_{unit\,cell}/(2 \times R_{La}{}^{3+} + R_{Ln}{}^{3+})$ Å$^2$), $La_2(Yb_{0.5}Nb_{0.5})_2O_7$ has a smaller value (195.68 Å$^2$) than that of $La_2(Dy_{0.5}Nb_{0.5})_2O_7$ (196.97 Å$^2$). Therefore, $La_2(Dy_{0.5}Nb_{0.5})_2O_7$ has a more open structure, which may result in a lower $T(\varepsilon_m)$. Thus, $NbO_6$ distortion appears to be an important factor to determine the $T(\varepsilon_m)$, nonetheless, it is clear that other factors such as normalized unit cell volume, dipole interactions and polarization may also play a role.

In summary, $La_2(Dy_{0.5}Nb_{0.5})_2O_7$ has the highest dielectric permittivity among the three compounds at all measured temperatures, $La_2(Er_{0.5}Nb_{0.5})_2O_7$ intermediate, and $La_2(Yb_{0.5}Nb_{0.5})_2O_7$ has the lowest value, which can be expected by the polarizability of $Ln'^{3+}$ ions. The temperature at which the maximum permittivity occurs are different, −132 °C for $La_2(Yb_{0.5}Nb_{0.5})_2O_7$, −197 °C for $La_2(Er_{0.5}Nb_{0.5})_2O_7$ and −187 °C for $La_2(Dy_{0.5}Nb_{0.5})_2O_7$.

## 4. Conclusion

The series of $La_2(Ln'_{0.5}Nb_{0.5})_2O_7$ compounds were synthesized by solid state processing. These compounds have an orthorhombic fluorite-related structure. $La_2(Yb_{0.5}Nb_{0.5})_2O_7$ is orthorhombic pyrochlore, and $La_2(Er_{0.5}Nb_{0.5})_2O_7$ and $La_2(Dy_{0.5}Nb_{0.5})_2O_7$ are weberite-type. Their dielectric properties were also investigated. The three compounds show temperature and frequency dependent dielectric relaxation. Arrhenius function was used to model the dielectric relaxation. The calculated attempt frequency is $1.2 \times 10^{14}$ Hz, $4.2 \times 10^{13}$ Hz and $1.82 \times 10^{12}$ Hz for $La_2(Yb_{0.5}Nb_{0.5})_2O_7$, $La_2(Er_{0.5}Nb_{0.5})_2O_7$ and $La_2(Dy_{0.5}Nb_{0.5})_2O_7$, respectively. The activation energy is 0.14 eV, 0.125 eV and 0.09 eV for $La_2(Yb_{0.5}Nb_{0.5})_2O_7$, $La_2(Er_{0.5}Nb_{0.5})_2O_7$ $La_2(Dy_{0.5}Nb_{0.5})_2O_7$, respectively. It is also found out that the $NbO_6$ distortion correlates with $T(\varepsilon_m)$.

## Acknowledgements

The authors would like to thank the Major Analytical Instrumentation Center (MAIC) at the University of Florida, and the financial support by the U.S. National Science Foundation for funding CAREER grant (DMR-0449710 and CBET 0730900).

## References

1. Cai, L. and Nino, J. C., Complex Ceramic Structures. 1. Weberites. *Acta Crystallographica Section B-Structural Science*, 2009, **B65**, 269–290.
2. Subramanian, M. A., Aravamudan, G. and Rao, G. V. S., Oxide pyrochlores—a review. *Progress in Solid State Chemistry*, 1983, **15**, 55–143.
3. Rossell, H. J., Fluorite-related phases $Ln_3MO_7$, Ln = rare-earth, Y or Sc, *M* = Nb, Sb, or Ta.2. Structure determination. *Journal of Solid State Chemistry*, 1979, **27**, 115–122.
4. Rooksby, H. P. and White, E. A. D., Rare-earth niobates and tantalates of defect fluorite-type and weberite-type structures. *Journal of the American Ceramic Society*, 1964, **47**, 94–96.
5. Sirotinkin, V. P., Evdokimov, A. A. and Trunov, V. K., Parameter improvement of nucleus of $Ln_3NbO_7$ and $Ln_3TaO_7$ compounds. *Zhurnal Neorganicheskoi Khimii*, 1982, **27**, 1648–1651.
6. Kovyazina, S. A., Perelyaeva, L. A., Leonidov, I. A. *et al.*, High-temperature structural disorder in $R_3NbO_7$. *Journal of Structural Chemistry*, 2003, **44**, 975–979.
7. Isupov, V. A., Oxide pyrochlores and their phase transitions. *Ferroelectrics Review*, 2000, **2**, 115–168.
8. Cai, L., Guzman, J., Perez, L. *et al.*, Phase formation and dielectric properties of $Ln_3NbO_7$ (Ln = rare earth elements). In *Solid-State Chemistry of Inorganic Materials VI (Materials Research Society Symposium Proceeding), vol. 998E*, 2007. pp. 0988-qq0901-0904.
9. Cai, L. and Nino, J. C., Structure and dielectric properties of $Ln_3NbO_7$ (Ln = Nd, Gd, Dy, Er, Yb and Y). *Journal of the European Ceramic Society*, 2007, **27**, 3971–3976.
10. Astafyev, A. V., Sirotinkin, V. P. and Stefanovich, S. Y., Phase-transitions in the compounds $Sm_3NbO_7$ and $Gd_3NbO_7$ with a fluorite-like structure. *Kristallografiya*, 1985, **30**, 603–604.
11. Cheary, R. W. and Coelho, A. A., Programs XFIT and FOURYA. *deposited in CCP14 Powder Diffraction Library*. Engineering and Physical Sciences Research Council, Daresbury Laboratory, Warrington, England, 1996.
12. Shirley, R., *The CRYSFIRE System for Automatic Powder Indexing*., 2004.
13. Laugier, J. and Bochu, B., *LMGP Suite for Windows - Checkcell*., 2004.
14. Fischer, M., Malcherek, T., Bismayer, U. *et al.*, Structure and stability of $Cd_2Nb_2O_7$ and $Cd_2Ta_2O_7$ explored by ab initio calculations. *Physical Review B*, 2008, **78**, 014108.
15. Ivanov, S., Tellgren, R. and Rundlof, H., Structural aspects of ferroelectric phase transitions in the complex metal oxides $A_2Sb_2O_7$ (A = Pb, Sr, Ca) with weberite structure. *Epdic*, 1998, **5**(Pts 1 and 2), 768–772, 278-2.
16. Cordfunke, E. H. P. and Ijdo, D. J. W., $Ba_2U_2O_7$—crystal-structure and phase-relationships. *Journal of Physics and Chemistry of Solids*, 1988, **49**, 551–554.
17. Lutterotti, L., Matthies, S. and Wenk, H.-R., MAUD: a friendly Java program for material analysis using diffraction. *IUCr: Newsletter of the CPD*, 1999, **21**, 14–15.

18. Roth, R. S., Vanderah, T. A., Bordet, P. *et al.*, Pyrochlore formation, phase relations, and properties in the $CaO\text{-}TiO_2\text{-}(Nb,Ta)_2O_5$ systems. *Journal of Solid State Chemistry*, 2008, **181**, 406–414.
19. Nino, J. C., Lanagan, M. T. and Randall, C. A., Dielectric relaxation in $Bi_2O_3\text{-}ZnO\text{-}Nb_2O_5$ cubic pyrochlore. *Journal of Applied Physics*, 2001, **89**, 4512–4516.
20. Nino, J. C., Lanagan, M. T., Randall, C. A. *et al.*, Correlation between infrared phonon modes and dielectric relaxation in Bi2O3-ZnO-Nb2O5 cubic pyrochlore. *Applied Physics Letters*, 2002, **81**, 4404–4406.
21. Kamba, S., Bovtun, V., Petzelt, J. *et al.*, Dielectric dispersion of the relaxer PLZT ceramics in the frequency range 20 Hz-100 THz. *Journal of Physics-Condensed Matter*, 2000, **12**, 497–519.
22. Binder, K. and Young, A. P., Spin glasses: experimental facts, theoretical concepts, and open questions. *Reviews of Modern Physics*, 1986, **58**, 801.
23. Bhattacharya, S., Nagel, S. R., Fleishman, L. *et al.*, Dielectric susceptibility of $(KBr)_{0.50}(KCN)_{0.50}$—is it a dipole glass. *Physical Review Letters*, 1982, **48**, 1267–1270.
24. Baur, W. H., Geometry of polyhedral distortions—predictive relationships for phosphate group. *Acta Crystallographica Section B-Structural Science B*, 1974, **30**, 1195–1215.
25. Shannon, R. D., Revised effective ionic-radii and systematic studies of interatomic distances in halides and chalcogenides. *Acta Crystallographica Section A*, 1976, **32**, 751–767.